



HAL
open science

Well-balanced finite difference WENO schemes for the blood flow model

Zhenzhen Wang, Gang Li, Olivier Delestre

► **To cite this version:**

Zhenzhen Wang, Gang Li, Olivier Delestre. Well-balanced finite difference WENO schemes for the blood flow model. *International Journal for Numerical Methods in Fluids*, 2016, 10.1002/flid.4232 . hal-01334841v2

HAL Id: hal-01334841

<https://hal.science/hal-01334841v2>

Submitted on 29 Jun 2016

HAL is a multi-disciplinary open access archive for the deposit and dissemination of scientific research documents, whether they are published or not. The documents may come from teaching and research institutions in France or abroad, or from public or private research centers.

L'archive ouverte pluridisciplinaire **HAL**, est destinée au dépôt et à la diffusion de documents scientifiques de niveau recherche, publiés ou non, émanant des établissements d'enseignement et de recherche français ou étrangers, des laboratoires publics ou privés.

Well-balanced finite difference WENO schemes for the blood flow model

Zhenzhen Wang^a, Gang Li^{a,*}, Olivier Delestre^b

^a School of Mathematics and Statistics, Qingdao University, Qingdao, Shandong 266071, P.R. China

^b Laboratory J.A. Dieudonné & EPU Nice Sophia, UMR 7351 Parc Valrose, 28 Avenue Valrose 06108 Nice
Cedex 02, 06000 Nice, France

Abstract

The blood flow model maintains the steady state solutions, in which the flux gradients are non-zero but exactly balanced by the source term. In this paper, we design high order finite difference weighted non-oscillatory (WENO) schemes to this model with such well-balanced property and at the same time keeping genuine high order accuracy. Rigorous theoretical analysis as well as extensive numerical results all indicate that the resulting schemes verify high order accuracy, maintain the well-balanced property, and keep good resolution for smooth and discontinuous solutions.

Keywords: Blood flow model; Finite difference schemes; WENO schemes; Well-balanced property; High order accuracy; Source term

1. Introduction

In this paper, we are interested in numerical simulation for the blood flow model by high order finite difference schemes. The numerical simulations with high order accuracy have a wide applications in medical engineering [1, 2]. As quoted by Xiu and Sherwin [3], the blood flow in arteries model was written long time ago by Leonhard Euler in 1775. However, the model is too difficult to solve [4]. Herein, for the sake of simplicity, we neglect the friction

*Corresponding author. Tel.: +86-0532-85953660. Fax: +86-0532-85953660.

Email addresses: wzz0667@163.com (Zhenzhen Wang), gangli1978@163.com (Gang Li), Delestre@unice.fr (Olivier Delestre)

term and consider the following governing equations

$$\begin{cases} \partial_t A + \partial_x Q = 0, \\ \partial_t Q + \partial_x \left(\frac{Q^2}{A} + \frac{k}{3\rho\sqrt{\pi}} A^{\frac{3}{2}} \right) = \frac{kA}{\rho\sqrt{\pi}} \partial_x (\sqrt{A_0}), \end{cases} \quad (1)$$

where A is the cross-sectional area ($A = \pi R^2$ with R being the radius of the vessel), $Q = Au$ denotes the discharge, u means the flow velocity, and ρ stands for the blood density. k represents the stiffness arterial. In addition, A_0 is the cross section at rest (*i.e.*, $A_0 = \pi R_0^2$ with R_0 being the radius of the vessel, which may be variable in the case of aneurism, stenosis or taper).

The blood flow model (1) with the source term are also called as *balance laws*. This model can admit the following steady state solutions, also called “man at eternal rest” (by analogy to the “lake at rest” in the shallow water equations)

$$u = 0, \quad A = A_0. \quad (2)$$

For the steady state solutions (2), the source term is exactly balanced by the non-zero flux gradient. Thus it is desirable to maintain the balance between the flux gradient and the source term at the discrete level. But such a balance is usually neither a constant nor a polynomial function. So standard numerical schemes usually fail to capture the steady state solutions well and may generally introduce spurious oscillations. The mesh must be extremely refined to reduce the size of these oscillations, but this strategy is impractical for multi-dimensional cases due to the high computational costs. Bermúdez and Vázquez [5] in 1994 proposed the idea of “exact conservation property”, which means that a scheme is exactly compatible with the steady state solutions. This property is also known as “well-balanced” property and is crucial for the balance between the flux gradient and the source term. An efficient scheme should satisfies this well-balanced property. Such schemes are often regarded as well-balanced schemes after the pioneering works of Greenberg et al. [6, 7]. The well-balanced schemes can preserve exactly these steady state solutions up to the machine error free of excessive mesh refinement and save computational cost accordingly. Moreover, the important advantage of well-balanced schemes over non-well-balanced schemes is that

they can accurately resolve small perturbations of such steady state solutions with relatively coarse meshes [8, 9]. More information about well-balanced schemes can be found in the lecture note [8]. Many researchers have developed well-balanced schemes for the shallow water equations admitting the still water steady state using different approaches, see, *e.g.*, [10–15] and the references therein. It is a challenging to design well-balanced schemes for the moving water equilibrium of the shallow water equations. Most well-balanced schemes for the still water steady state cannot preserve the moving water equilibrium automatically. A few attempts can be found in [16–18]. In addition, the research of the well-balanced schemes for the Euler equations under gravitational fields is also an active subject [19–24].

In recent years, there have been many interesting attempts proposed in the literature to derive well-balanced schemes for the blood flow model. For example, Delestre *et al.* [25] present a well-balanced finite volume scheme for the blood flow model based on the conservative governing equations [27–29]. Recently, Müller *et al.* [30] constructed a well-balanced high order finite volume for the blood flow in elastic vessels with varying mechanical properties. More recently, Murillo *et al.* [31] present an energy-balanced approximate solver for the blood flow model with upwind discretization for the source term.

The main objective of this paper is to design a well-balanced finite difference weighted non-oscillatory (WENO) scheme which maintains the well-balanced property and at the same time keeps genuinely high order accuracy for the general solutions of the blood flow model, based on a special splitting of the source term into two parts which are discretized separately.

This paper is organized as follows: in Section 2, we propose a high order well-balanced finite difference WENO scheme. Extensive numerical experiments are carried out in Section 3. Conclusions are given in Section 4.

2. Well-balanced WENO schemes

In this section, we present high order well-balanced WENO schemes for the blood flow model satisfying the steady state solution (2).

2.1. Notations

For simplicity, we assume that the grid points $\{x_j\}$ are uniformly distributed with cell size $\Delta x = x_{j+1} - x_j$ and we denote the cells by $I_j = [x_{j-1/2}, x_{j+1/2}]$ with $x_{j+1/2} = x_j + \Delta x/2$ as the center of the cell I_j .

2.2. A review of finite difference WENO schemes

The first finite difference WENO scheme was designed in 1996 by Jiang and Shu [32] for hyperbolic conservation laws. More detailed information of WENO schemes can be found in the lecture note [33]. For the latest advances regarding WENO schemes, we refer to the review [34]. We begin with the description for the 1D scalar conservation laws

$$u_t + f(u)_x = 0. \quad (3)$$

High order semi-discrete conservative finite difference schemes of (3) can be formulated as follows

$$\frac{d}{dt}u_j(t) = -\frac{1}{\Delta x} \left(\hat{f}_{j+1/2} - \hat{f}_{j-1/2} \right), \quad (4)$$

where $u_j(t)$ is the numerical approximation to the point value $u(x_j, t)$, and the numerical flux $\hat{f}_{j+1/2}$ is used to approximate $h_{j+1/2} = h(x_{j+1/2})$ with high order accuracy. Here $h(x)$ is implicitly defined as in [32]

$$f(u(x)) = \frac{1}{\Delta x} \int_{x-\Delta x/2}^{x+\Delta x/2} h(\xi) d\xi.$$

We take upwinding into account to maintain the numerical stability and splitting a general flux into two parts

$$f(u) = f^+(u) + f^-(u),$$

where $\frac{df^+(u)}{du} \geq 0$ and $\frac{df^-(u)}{du} \leq 0$. One example is the simple Lax-Friedrichs flux

$$f^\pm(u) = \frac{1}{2}(f(u) \pm \alpha u), \quad (5)$$

where $\alpha = \max_u |\lambda(u)|$ with $\lambda(u)$ being the eigenvalues of the Jacobian $f'(u)$, and the maximum is taken over the whole region. With respect to $f^+(u)$ and $f^-(u)$, we can get numerical

fluxes $\hat{f}_{j+1/2}^+$ and $\hat{f}_{j+1/2}^-$ using the WENO reconstruction, respectively. Finally, we get the numerical fluxes as follows

$$\hat{f}_{j+1/2} = \hat{f}_{j+1/2}^+ + \hat{f}_{j+1/2}^-.$$

By means of the WENO approximation procedure, $\hat{f}_{j+1/2}^+$ is expressed as [32]

$$\hat{f}_{j+1/2}^+ = \sum_{k=0}^r \omega_k q_k^r (f_{j+k-r}^+, \dots, f_{j+k}^+), \quad (6)$$

where ω_k is the nonlinear weight, $f_i^+ = f^+(u_i)$, $i = j - r, \dots, j + r$, and

$$q_k^r (g_0, \dots, g_r) = \sum_{l=0}^r a_{k,l}^r g_l \quad (7)$$

is the low order approximation to $\hat{f}_{j+1/2}^+$ on the k th stencil $S_k = (x_{j+k-r}, \dots, x_{j+k})$, $k = 0, 1, \dots, r$, and $a_{k,l}^r$, $0 \leq k, l \leq r$ are constant coefficients, see [33] for more details.

The nonlinear weights ω_k in (6) satisfy

$$\sum_{k=0}^r \omega_k = 1,$$

and are designed to yield $(2r + 1)$ th-order accuracy in smooth regions of the solution. In [32, 33], the nonlinear weight ω_k is formulated as

$$\omega_k = \frac{\alpha_k}{\sum_{l=0}^r \alpha_l}, \quad \text{with } \alpha_k = \frac{C_k^r}{(\varepsilon_{\text{WENO}} + IS_k)^2}, \quad k = 0, 1, \dots, r, \quad (8)$$

where C_k^r is the linear weight. IS_k is a smoothness indicator of $f^+(u)$ on stencil S_k , $k = 0, 1, \dots, r$, and $\varepsilon_{\text{WENO}}$ is a small constant used here to avoid the denominator becoming zero, $\varepsilon_{\text{WENO}} = 10^{-6}$ is used in all test cases in this paper. We employed the smoothness indicators proposed in [32, 33], *i.e.*,

$$IS_k = \sum_{l=1}^r \int_{x_{j-1/2}}^{x_{j+1/2}} (\Delta x)^{2l-1} \left(q_k^{(l)} \right)^2 dx,$$

where $q_k^{(l)}$ is the l th-derivative of $q_k(x)$ which is the reconstruction polynomial of $f^+(u)$ on stencil S_k such that

$$\frac{1}{\Delta x} \int_{I_i} q_k(x) dx = f_i^+, \quad i = j + k - r, \dots, j + k.$$

The WENO approximation procedure for $\hat{f}_{j+\frac{1}{2}}^-$ is a mirror symmetry to that of $\hat{f}_{j+\frac{1}{2}}^+$ with respect to $x_{j+1/2}$.

Consequently, the numerical flux $\hat{f}_{j+1/2}$ is then calculated by

$$\hat{f}_{j+1/2} = \hat{f}_{j+1/2}^+ + \hat{f}_{j+1/2}^-.$$

Ultimately, we obtain the semi-discrete scheme (4).

2.3. Well-balanced WENO schemes for the blood flow model

In order to design well-balanced schemes, we firstly split the source term $\frac{kA}{\rho\sqrt{\pi}}\partial_x(\sqrt{A_0})$ into two terms $\frac{k}{\rho\sqrt{\pi}}(A - A_0)\partial_x(\sqrt{A_0}) + \frac{k}{3\rho\sqrt{\pi}}\partial_x\left(A_0^{\frac{3}{2}}\right)$ in a equivalent form. Therefore the original system (1) becomes

$$\begin{cases} \partial_t A + \partial_x Q = 0, \\ \partial_t Q + \partial_x \left(\frac{Q^2}{A} + \frac{k}{3\rho\sqrt{\pi}} A^{\frac{3}{2}} \right) = \frac{k}{\rho\sqrt{\pi}}(A - A_0)\partial_x(\sqrt{A_0}) + \frac{k}{3\rho\sqrt{\pi}}\partial_x \left(A_0^{\frac{3}{2}} \right), \end{cases} \quad (9)$$

which can be denoted in a compact vector form

$$U_t + f(U)_x = S_1 + S_2,$$

where $U = (A, Q)^T$, $f(U) = \left(Q, \frac{Q^2}{A} + \frac{k}{3\rho\sqrt{\pi}} A^{\frac{3}{2}} \right)$, $S_1 = \left(0, \frac{k}{\rho\sqrt{\pi}}(A - A_0)\partial_x(\sqrt{A_0}) \right)^T$ and $S_2 = \left(0, \frac{k}{3\rho\sqrt{\pi}}\partial_x \left(A_0^{\frac{3}{2}} \right) \right)^T$.

Subsequently, we consider a numerical scheme for solving (9). The scheme may be classified as a *linear scheme*, because all of the spatial derivatives are approximated by a linear finite difference operator D that is defined to satisfy

$$D(\alpha f + \beta g) = \alpha D(f) + \beta D(g) \quad (10)$$

for any constants α, β and grid functions f and g .

For such a linear scheme, we have

Proposition 1. *A linear scheme for the 1D blood flow model satisfying the steady state solutions (2) can maintain the well-balanced property.*

Proof. For the steady state solutions (2), linear schemes satisfying (10) are exact for the first equation $\partial_x Q = 0$, since $Q = 0$ due to $u = 0$, and the truncation error for the second equation reduces to

$$\begin{aligned} & D\left(\frac{Q^2}{A} + \frac{k}{3\rho\sqrt{\pi}}A^{\frac{3}{2}}\right) - \frac{k}{\rho\sqrt{\pi}}(A - A_0)D(\sqrt{A_0}) + \frac{k}{3\rho\sqrt{\pi}}D\left(A_0^{\frac{3}{2}}\right) \\ &= D\left(\frac{k}{3\rho\sqrt{\pi}}A^{\frac{3}{2}} - \frac{k}{3\rho\sqrt{\pi}}A_0^{\frac{3}{2}}\right) \\ &= 0, \end{aligned}$$

where the first equality thanks to the facts that $Q = 0$ due to $u = 0$ and $A = A_0$ as well as the linearity of the finite difference operator D ; the second one is also due to the fact that $A = A_0$ and the consistency of the finite difference operator D . As a consequence, this finishes the proof. \square

However, the WENO schemes are nonlinear. The nonlinearity comes from the nonlinear weight, which in turn comes from the nonlinearity of the smoothness indicators. In order to construct a linear scheme which can maintain the well-balanced property even with the presence of the nonlinearity of the nonlinear weight and does not affect the high-order accuracy, we must take some modifications.

To present the basic ideas of the modification, we firstly consider the situation when the WENO scheme is applied without the flux splitting and the local characteristic decomposition.

Before considering an approximation of the flux gradient $f(U)_x$, we must firstly reconstruct the numerical flux $\hat{f}_{j+1/2}$. We consider a WENO scheme with a global Lax-Friedrichs flux splitting, denoted by the WENO-LF scheme. Now the flux $f(U)$ writes

$$f(U) = f^+(U) + f^-(U),$$

where

$$f^\pm(U) = \frac{1}{2} \left[\begin{pmatrix} Q \\ \frac{Q^2}{A} + \frac{k}{3\rho\sqrt{\pi}}A^{\frac{3}{2}} \end{pmatrix} \pm \alpha_i \begin{pmatrix} A \\ Q \end{pmatrix} \right], \quad (11)$$

with

$$\alpha_i = \max_u |\lambda_i(u)| \quad (12)$$

for the i th characteristic field, where $\alpha_i = \max_u |\lambda_i(u)|$ with $\lambda_i(u)$ being the i th eigenvalue of the Jacobian $f'(U)$. In order to design a linear finite difference operator, we adopt a minor modification to the flux splitting by replacing $\pm\alpha_i \begin{pmatrix} A \\ Q \end{pmatrix}$ in (11) with $\pm\alpha_i \begin{pmatrix} A - A_0 \\ Q \end{pmatrix}$.

So the flux splitting (11) now becomes

$$f^\pm(U) = \frac{1}{2} \left[\begin{pmatrix} Q \\ \frac{Q^2}{A} + \frac{k}{3\rho\sqrt{\pi}} A^{\frac{3}{2}} \end{pmatrix} \pm \alpha_i \begin{pmatrix} A - A_0 \\ Q \end{pmatrix} \right]. \quad (13)$$

This modification is justified by the fact that A_0 is independent of time t .

Provided $\hat{f}_{j+1/2} = \hat{f}_{j+1/2}^+ + \hat{f}_{j+1/2}^-$ based on the WENO approximation procedure using the modified flux splitting (13), the flux gradient $f(U)_x$ may be finally approximated by

$$f(U)_x|_{x=x_j} \approx \frac{\hat{f}_{j+1/2} - \hat{f}_{j-1/2}}{\Delta x}.$$

Herein, in order to achieve a more accurate solution at the price of more complicated computations, the WENO approximation is implemented with a local characteristic decomposition procedure, see [33] for more details.

Subsequently, the WENO-LF schemes can be demonstrated to maintain the steady state solutions (2), *i.e.*, to satisfy the well-balanced property.

Firstly, $\hat{f}_{j+1/2}^+$ is given by

$$\begin{aligned} \hat{f}_{j+1/2}^+ &= \sum_{k=-r}^r c_k f_{j+k}^+ \\ &= \sum_{k=-r}^r c_k \frac{1}{2} (f_{j+k} + \alpha U_{j+k}) \\ &= \frac{1}{2} \sum_{k=-r}^r c_k f_{j+k} + \frac{1}{2} \sum_{k=-r}^r c_k (\alpha U_{j+k}), \end{aligned} \quad (14)$$

where $f^+ = f^+(U)$ is defined in (13) with $U = (A - A_0, Q)^T$ and $f = f(U) = \left(Q, \frac{Q^2}{A} + \frac{k}{3\rho\sqrt{\pi}} A^{\frac{3}{2}} \right)^T$ being the vector grid functions, c_k is a 2×2 matrix depending nonlinearly on the smoothness indicators of f^+ on the stencil $\{x_{j-r}, \dots, x_{j+r}\}$, and α is a 2×2 diagonal matrix involving α_i in (12).

Similarly, $\hat{f}_{j+1/2}^-$ can be written as

$$\begin{aligned}
\hat{f}_{j+1/2}^- &= \sum_{k=-r+1}^{r+1} a_k f_{j+k}^- \\
&= \sum_{k=-r+1}^{r+1} a_k \frac{1}{2} (f_{j+k} - \alpha U_{j+k}) \\
&= \frac{1}{2} \sum_{k=-r+1}^{r+1} a_k f_{j+k} - \frac{1}{2} \sum_{k=-r+1}^{r+1} a_k (\alpha U_{j+k}),
\end{aligned} \tag{15}$$

where $f^- = f^-(U)$. As c_k in (14), herein a_k is also a 2×2 matrix but depending nonlinearly on the smoothness indicators of f^- on the stencil $\{x_{j-r+1}, \dots, x_{j+r+1}\}$, and α is a 2×2 diagonal matrix involving α_i in (12).

Ultimately, we have

$$\begin{aligned}
\hat{f}_{j+1/2} &= \hat{f}_{j+1/2}^+ + \hat{f}_{j+1/2}^- \\
&= \frac{1}{2} \sum_{k=-r}^r c_k f_{j+k} + \frac{1}{2} \sum_{k=-r}^r c_k (\alpha U_{j+k}) + \frac{1}{2} \sum_{k=-r+1}^{r+1} a_k f_{j+k} - \frac{1}{2} \sum_{k=-r+1}^{r+1} a_k (\alpha U_{j+k}).
\end{aligned} \tag{16}$$

Likewise, $\hat{f}_{j-1/2}^+$ and $\hat{f}_{j-1/2}^-$ can be defined. So, we can obtain $\hat{f}_{j-1/2}$ as follows

$$\begin{aligned}
\hat{f}_{j-1/2} &= \hat{f}_{j-1/2}^+ + \hat{f}_{j-1/2}^- \\
&= \frac{1}{2} \sum_{k=-r-1}^{r-1} \hat{c}_k f_{j+k} + \frac{1}{2} \sum_{k=-r-1}^{r-1} \hat{c}_k (\alpha U_{j+k}) + \frac{1}{2} \sum_{k=-r}^r \hat{a}_k f_{j-k} - \frac{1}{2} \sum_{k=-r}^r \hat{a}_k (\alpha U_{j-k}).
\end{aligned} \tag{17}$$

Herein, \hat{c}_k is a 2×2 matrix depending nonlinearly on the smoothness indicators of f^+ on the stencil $\{x_{j-r-1}, \dots, x_{j+r-1}\}$. \hat{a}_k is also a 2×2 matrix depending nonlinearly on the smoothness indicators of f^- on the stencil $\{x_{j-r}, \dots, x_{j+r}\}$.

Subsequently, the approximation to $f(U)_x$ can be obtained as follows

$$\begin{aligned}
f(U)_x|_{x=x_j} &\approx \frac{1}{\Delta x} \left(\hat{f}_{j+1/2} - \hat{f}_{j-1/2} \right) \\
&= \frac{1}{\Delta x} \left[\left(\frac{1}{2} \sum_{k=-r}^r c_k f_{j+k} + \frac{1}{2} \sum_{k=-r}^r c_k (\alpha U_{j+k}) + \frac{1}{2} \sum_{k=-r+1}^{r+1} a_k f_{j+k} - \frac{1}{2} \sum_{k=-r+1}^{r+1} a_k (\alpha U_{j+k}) \right) \right. \\
&\quad \left. - \left(\frac{1}{2} \sum_{k=-r-1}^{r-1} \hat{c}_k f_{j+k} + \frac{1}{2} \sum_{k=-r-1}^{r-1} \hat{c}_k (\alpha U_{j+k}) + \frac{1}{2} \sum_{k=-r}^r \hat{a}_k f_{j-k} - \frac{1}{2} \sum_{k=-r}^r \hat{a}_k (\alpha U_{j-k}) \right) \right] \\
&= \frac{1}{2\Delta x} \left(\sum_{k=-r}^r c_k f_{j+k} - \sum_{k=-r-1}^{r-1} \hat{c}_k f_{j+k} \right) \\
&\quad + \frac{1}{2\Delta x} \left(\sum_{k=-r+1}^{r+1} a_k f_{j+k} - \sum_{k=-r}^r \hat{a}_k f_{j-k} \right) \\
&\quad + \frac{1}{2\Delta x} \left(\sum_{k=-r}^r c_k (\alpha U_{j+k}) - \sum_{k=-r-1}^{r-1} \hat{c}_k (\alpha U_{j+k}) \right) \\
&\quad + \frac{1}{2\Delta x} \left(\sum_{k=-r}^r \hat{a}_k (\alpha U_{j-k}) - \sum_{k=-r+1}^{r+1} a_k (\alpha U_{j+k}) \right).
\end{aligned} \tag{18}$$

It should be noted that with $\pm \alpha U = \pm \alpha (A - A_0, Q)^T$ instead of $\pm \alpha (A, Q)^T$ in the flux splitting (11), the first two terms on the right hand side of the above expression become constant vectors for the steady state solutions (2). Denoting U_{j+k} as U for simplicity, we have $\alpha U_{j+k} = \alpha U$ as a constant vector. Consequently

$$\begin{aligned}
&\frac{1}{2\Delta x} \left(\sum_{k=-r}^r c_k (\alpha U_{j+k}) - \sum_{k=-r-1}^{r-1} \hat{c}_k (\alpha U_{j+k}) \right) \\
&= \frac{1}{2\Delta x} \left(\sum_{k=-r}^r c_k (\alpha U) - \sum_{k=-r-1}^{r-1} \hat{c}_k (\alpha U) \right) \\
&= \frac{1}{2\Delta x} \left[\left(\sum_{k=-r}^r c_k \right) (\alpha U) - \left(\sum_{k=-r-1}^{r-1} \hat{c}_k \right) (\alpha U) \right] \\
&= \frac{1}{2\Delta x} [I \cdot (\alpha U) - I \cdot (\alpha U)] \\
&= 0,
\end{aligned} \tag{19}$$

where I is a 2×2 identity matrix, the identities $\sum_{k=-r}^r c_k = I$ and $\sum_{k=-r-1}^{r-1} \hat{c}_k = I$ are due to the consistency of the WENO approximation. Similarly, we have

$$\frac{1}{2\Delta x} \left(\sum_{k=-r}^r \hat{a}_k (\alpha U_{j-k}) - \sum_{k=-r+1}^{r+1} a_k (\alpha U_{j+k}) \right) = 0. \tag{20}$$

Finally, the approximation to $f(U)_x$ in (18) can be written as

$$\begin{aligned}
f(U)_x|_{x=x_j} &\approx \frac{1}{\Delta x} \left(\hat{f}_{j+1/2} - \hat{f}_{j-1/2} \right) \\
&= \frac{1}{2\Delta x} \left(\sum_{k=-r}^r c_k f_{j+k} - \sum_{k=-r-1}^{r-1} \hat{c}_k f_{j+k} \right) \\
&+ \frac{1}{2\Delta x} \left(\sum_{k=-r+1}^{r+1} a_k f_{j+k} - \sum_{k=-r}^r \hat{a}_k f_{j-k} \right) \\
&= \sum_{k=-r-1}^{r+1} \beta_k f_{j+k} \\
&\equiv D_f(f)_j,
\end{aligned} \tag{21}$$

where β_k is a 2×2 matrix depending on the smoothness indicators involving f^+ and f^- . Motivated by the research work in [14], the key idea of the current scheme is to apply the finite difference operator D_f , with the smoothness indicators and the coefficient matrix β_k in (21) fixed, to approximate the source terms $(0, \sqrt{A_0})_x^T$ and $(0, A_0^{\frac{3}{2}})_x^T$. This leads to the splitting of the two derivatives as

$$\begin{pmatrix} 0 \\ \sqrt{A_0} \end{pmatrix}_x = \frac{1}{2} \begin{pmatrix} 0 \\ \sqrt{A_0} \end{pmatrix}_x + \frac{1}{2} \begin{pmatrix} 0 \\ \sqrt{A_0} \end{pmatrix}_x, \quad \begin{pmatrix} 0 \\ A_0^{\frac{3}{2}} \end{pmatrix}_x = \frac{1}{2} \begin{pmatrix} 0 \\ A_0^{\frac{3}{2}} \end{pmatrix}_x + \frac{1}{2} \begin{pmatrix} 0 \\ A_0^{\frac{3}{2}} \end{pmatrix}_x, \tag{22}$$

which is handled by applying the similar flux splitting WENO approximation procedure. The two parts of each source term are approximated by the finite difference operator D_f with coefficients obtained from the computation of $f^+(U)$ and $f^-(U)$, respectively.

A key observation is that the finite difference operator D_f in (21), with the fixed coefficient matrix β_k , is a *linear* finite difference operator on any grid function as in (10). In addition, the finite difference operator D_f is a high order accurate *linear* approximation to the first derivative of a grid function. Therefore based on the Proposition 1, it may be proved that the WENO scheme with the modified flux splitting (13) and with the special handling of the source terms described in (22) maintains the well-balanced property. This leads to

Proposition 2. *The WENO-LF scheme for the blood flow model satisfying the steady state solutions (2) can maintain the well-balanced property without adverse effect on its original high order accuracy.*

For the temporal discretization, high order total variation diminishing (TVD) Runge-Kutta methods [35] can be used. In the numerical section of this paper, we apply the third order Runge-Kutta methods:

$$\begin{aligned} U^{(1)} &= U^n + \Delta t \mathcal{F}(U^n), \\ U^{(2)} &= \frac{3}{4}U^n + \frac{1}{4}(U^{(1)} + \Delta t \mathcal{F}(U^{(1)})), \\ U^{n+1} &= \frac{1}{3}U^n + \frac{2}{3}(U^{(2)} + \Delta t \mathcal{F}(U^{(2)})), \end{aligned} \tag{23}$$

with $\mathcal{F}(U)$ being the spatial operator.

3. Numerical results

In this section, we carry out extensive numerical experiments inspired by Delestre *et al.* [25] to demonstrate the performances of a fifth-order ($r = 2$) finite difference WENO scheme. The CFL number is taken as 0.6, except for the accuracy tests where smaller time step is taken to ensure that spatial errors dominate.

3.1. The ideal tourniquet

This example is similar to the Stoke's dam break problem in shallow water equations [26]. Herein, we consider the analogous problem in blood flow model: a tourniquet is applied and we remove it instantaneously. And we consider the following initial conditions

$$A(x, 0) = \begin{cases} \pi R_L^2 & \text{if } x \leq 0, \\ \pi R_R^2 & \text{otherwise,} \end{cases} \quad \text{and } Q(x, 0) = 0,$$

on a computational domain $[-0.04, 0.04]$ based on the following parameters: $k = 1. \times 10^7 Pa/m$, $\rho = 1060 kg/m^3$, $R_L = 5 \times 10^{-3} m$, $R_R = 4 \times 10^{-3} m$.

We solve this example on the mesh with 200 cells up to $t = 0.005$ s and present the numerical solutions against the exact ones in Fig. 1. It is clear that the numerical results fit well with the exact ones and keep steep shock transitions.

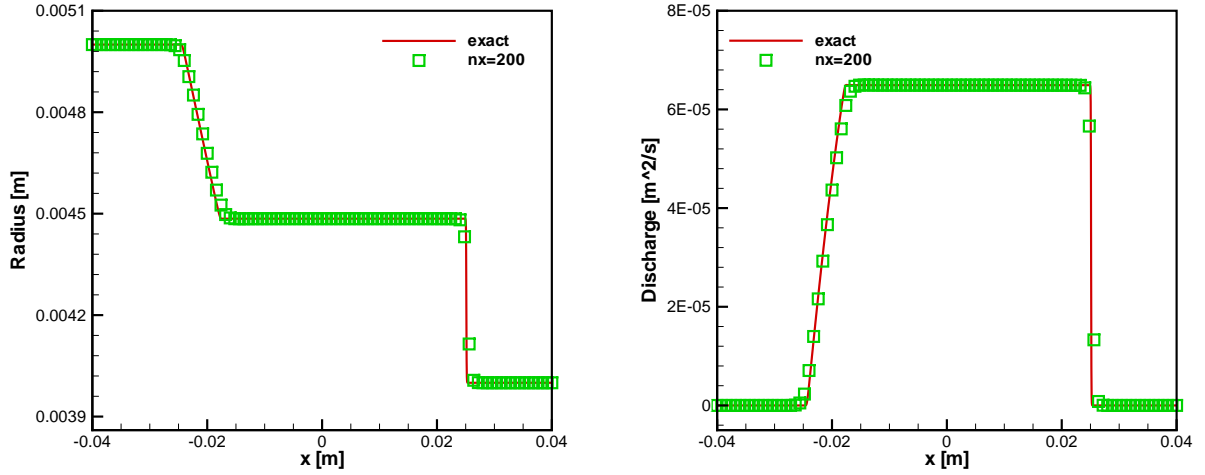


Fig. 1: The numerical solutions of the ideal tourniquet problem in Section 3.1 with 200 cells at $t = 0.005$ s. Radius (left) and discharge (right).

3.2. Wave equation

Then, the following quasi-stationary test case was proposed by Delestre *et al.* [25]. It is chosen to demonstrate the capability of the proposed scheme for computations on the perturbation of a steady state solutions. The initial conditions are given by

$$A(x, 0) = \begin{cases} \pi R_0^2 & \text{if } x \in [0, \frac{40L}{100}] \cup [\frac{60L}{100}, L], \\ \pi R_0^2 \left[1 + \epsilon \sin \left(\pi \frac{x - 40L/100}{20L/100} \right) \right]^2 & \text{if } x \in [\frac{40L}{100}, \frac{60L}{100}], \end{cases} \quad \text{and } Q(x, 0) = 0,$$

on the computational domain $[0, 0.16]$. The following parameters have been used for the example: $\epsilon = 5 \times 10^{-3}$, $k = 10^8$ Pa/m, $\rho = 1060$ kg/m³, $R_0 = 4 \times 10^{-3}$ m and $L = 0.16$ m.

With the above initial conditions, we obtain the following exact solutions:

$$\begin{cases} R(x, t) = R_0 + \frac{\epsilon}{2} [\Phi(x - c_0 t) + \Phi(x + c_0 t)], \\ u(x, t) = -\frac{\epsilon c_0}{2 R_0} [-\Phi(x - c_0 t) + \Phi(x + c_0 t)]. \end{cases}$$

We show the numerical solutions on a mesh with 200 cells at $t = 0.002$ s, 0.004 s, and 0.006 s, respectively in Fig. 2. The figure strongly suggests that the numerical solutions agree with the exact ones well. Moreover, we also test the orders of the resulting scheme by plotting the numerical errors at $t = 0.004$ s and show the L^1 errors as well as order of accuracy for A and Q in Table 1. It is evident that the expected fifth order accuracy has been achieved.

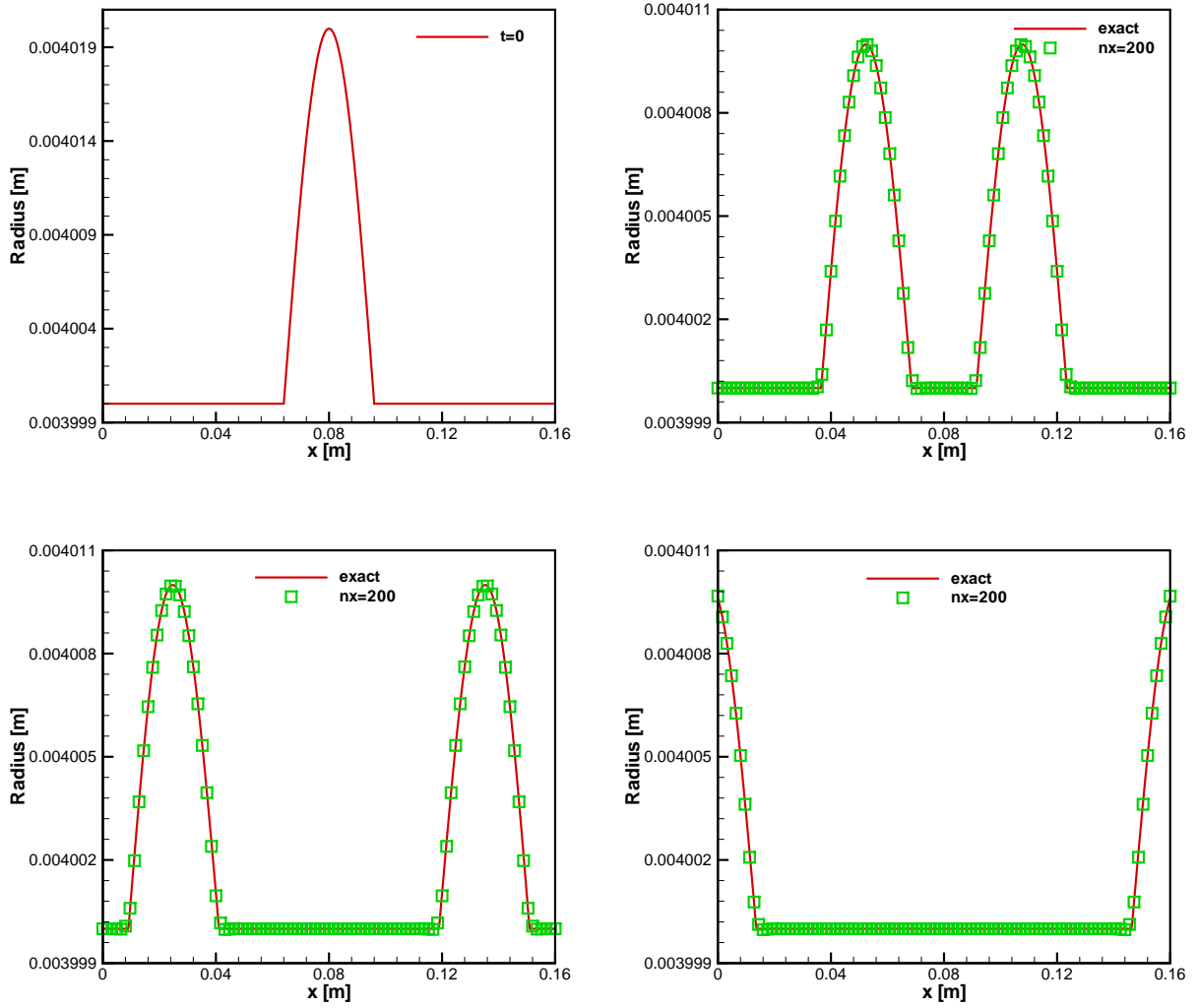


Fig. 2: The numerical solutions of the wave equation problem in Section 3.2 with 200 cells. Radius at time $t = 0$ s (upper left), $t = 0.002$ s (upper right), $t = 0.004$ s (lower left), and $t = 0.006$ s (lower right), respectively.

Table 1: L^1 errors and numerical orders of accuracy for the wave equation example of Section 3.2.

N	A		Q	
	L^1 error	Order	L^1 error	Order
25	1.7566E-02		1.0990E-01	
50	2.2028E-03	3.00	1.9714E-02	2.48
100	3.3138E-04	2.73	2.8273E-03	2.80
200	2.3271E-05	3.83	2.0103E-04	3.81
400	9.3899E-07	4.63	8.7320E-06	4.52
800	3.1516E-08	4.90	3.7319E-07	4.55
1600	9.1264E-10	5.11	1.1501E-08	5.02

3.3. The man at eternal rest

The purpose of this example is to verify that the scheme indeed maintains the well-balanced property.

Herein, we consider a configuration with no flow and with a change of radius $R_0(x)$, this is the case for a dead man with an aneurism. Thus, for the initial conditions, the section of the artery is not constant with the following form

$$R(x, 0) = R_0(x) = \begin{cases} \tilde{R} & \text{if } x \in [0, x_1] \cup [x_4, L], \\ \tilde{R} + \frac{\Delta R}{2} \left[\sin \left(\frac{x-x_1}{x_2-x_1} \pi - \frac{\pi}{2} \right) + 1 \right] & \text{if } x \in [x_1, x_2], \\ \tilde{R} + \Delta R & \text{if } x \in [x_2, x_3], \\ \tilde{R} + \frac{\Delta R}{2} \left[\cos \left(\frac{x-x_3}{x_4-x_3} \pi \right) + 1 \right] & \text{if } x \in [x_3, x_4], \end{cases}$$

on the computational domain $[0, L]$ with $\tilde{R} = 4. \times 10^{-3} m$, $\Delta R = 10^{-3} m$, $k = 10^8 Pa/m$, $\rho = 1060 kg/m^3$, $L = 0.14 m$, $x_1 = 10^{-2} m$, $x_2 = 3.05 \times 10^{-2} m$, $x_3 = 4.95 \times 10^{-2} m$ and $x_4 = 7. \times 10^{-2} m$. In addition, the initial velocity is zero. We compute this example up to $t = 5 s$.

In order to show that the well-balanced property is maintained up to machine round off error, tests are run using single, double and quadruple precisions, respectively. The L^1 and L^∞ errors calculated for A and Q are presented in Table 2. It can be clearly seen that the L^1 and L^∞ errors are all at the level of round off error associated with different precisions,

Table 2: L^1 and L^∞ errors for different precisions for the man at eternal rest.

Precision	L^1 error		L^∞ error	
	A	Q	A	Q
Single	3.47e-07	3.13e-07	3.54e-07	3.25e-07
Double	2.72e-16	4.34e-16	2.11e-15	3.14e-16
Quadruple	2.31e-33	4.34e-32	1.28e-33	2.44e-31

which verify that the current scheme maintains the well-balanced property as expected.

In Fig. 3, we present the radius at $t = 5$ s on a mesh with 200 cells against a reference solution obtained with a much refined 2000 cells. In addition, we run the same numerical test using the non-well-balanced WENO schemes, with a straightforward integration of the source term, and show their results in Fig. 3 for comparison. It is obvious that the results of the well-balanced WENO scheme are in good agreement with the reference solutions for the case, while the non-well-balanced WENO scheme fails to capture the small perturbation with 200 cells.

3.4. Propagation of a pulse to an expansion

Firstly, we test the case of a pulse in a section R_R passing through an expansion: $A_L > A_R$, taking the following parameters: $k = 1.0 \times 10^8$ Pa/m, $L = 0.16$ m, $\rho = 1060$ kg/m³, $R_L = 5 \times 10^{-3}$ m, $R_R = 4 \times 10^{-3}$ m, $\Delta R = 1.0 \times 10^{-3}$ m. We take a decreasing shape on a rather small scale:

$$R_0(x) = \begin{cases} R_R + \Delta R & \text{if } x \in [0, x_1], \\ R_R + \frac{\Delta R}{2} \left[1 + \cos \left(\frac{x-x_1}{x_2-x_1} \pi \right) \right] & \text{if } x \in [x_1, x_2], \\ R_R & \text{else,} \end{cases}$$

with $x_1 = \frac{19L}{40}$, $x_2 = \frac{L}{2}$. As initial conditions, we consider a fluid at rest $Q(x, 0) = 0$ m³/s and the following perturbation of radius:

$$R(x, 0) = \begin{cases} R_0(x) \left[1 + \epsilon \sin \left(\frac{100}{20L} \pi \left(x - \frac{65L}{100} \right) \right) \right] & \text{if } x \in \left[\frac{65L}{100}, \frac{85L}{100} \right], \\ R_0(x) & \text{else,} \end{cases}$$

with $\epsilon = 5.0 \times 10^{-3}$.

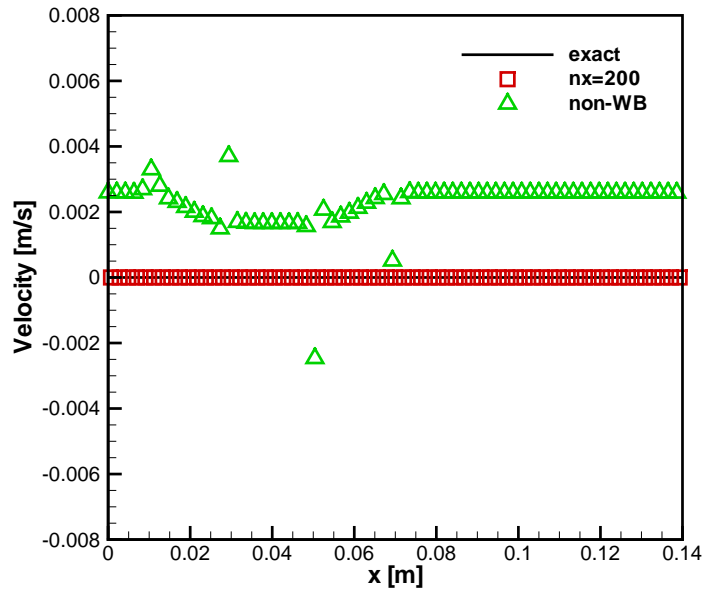


Fig. 3: The man at eternal rest problem in Section 3.3 with 200 cells at $t = 5$ s. The result of the well-balanced scheme with 200 and 2000 cells, and that of the non-well-balanced (denoted by non-WB) scheme with 200 cells.

In Fig. 4, we present the numerical results against the reference solutions at $t = 0.002$ s and $t = 0.006$ s. The numerical solutions are in good agreement with the reference ones and are comparable with those in [25].

3.5. Propagation of a pulse from an expansion

Then, we consider a pulse propagating from an expansion. So, the parameters are the same as in the Section 3.4, only the initial radius is changed:

$$R(x, 0) = \begin{cases} R_0(x) \left[1 + \epsilon \sin \left(\frac{100}{20L} \pi \left(x - \frac{15L}{100} \right) \right) \right] & \text{if } x \in \left[\frac{15L}{100}, \frac{35L}{100} \right], \\ R_0(x) & \text{else,} \end{cases}$$

with $\epsilon = 5.0 \times 10^{-3}$.

In Fig. 5, we demonstrate the numerical results against the reference solutions at $t = 0.002$ s and $t = 0.006$ s. Similar, the numerical solutions fit well with the reference ones and are comparable with those in [25].

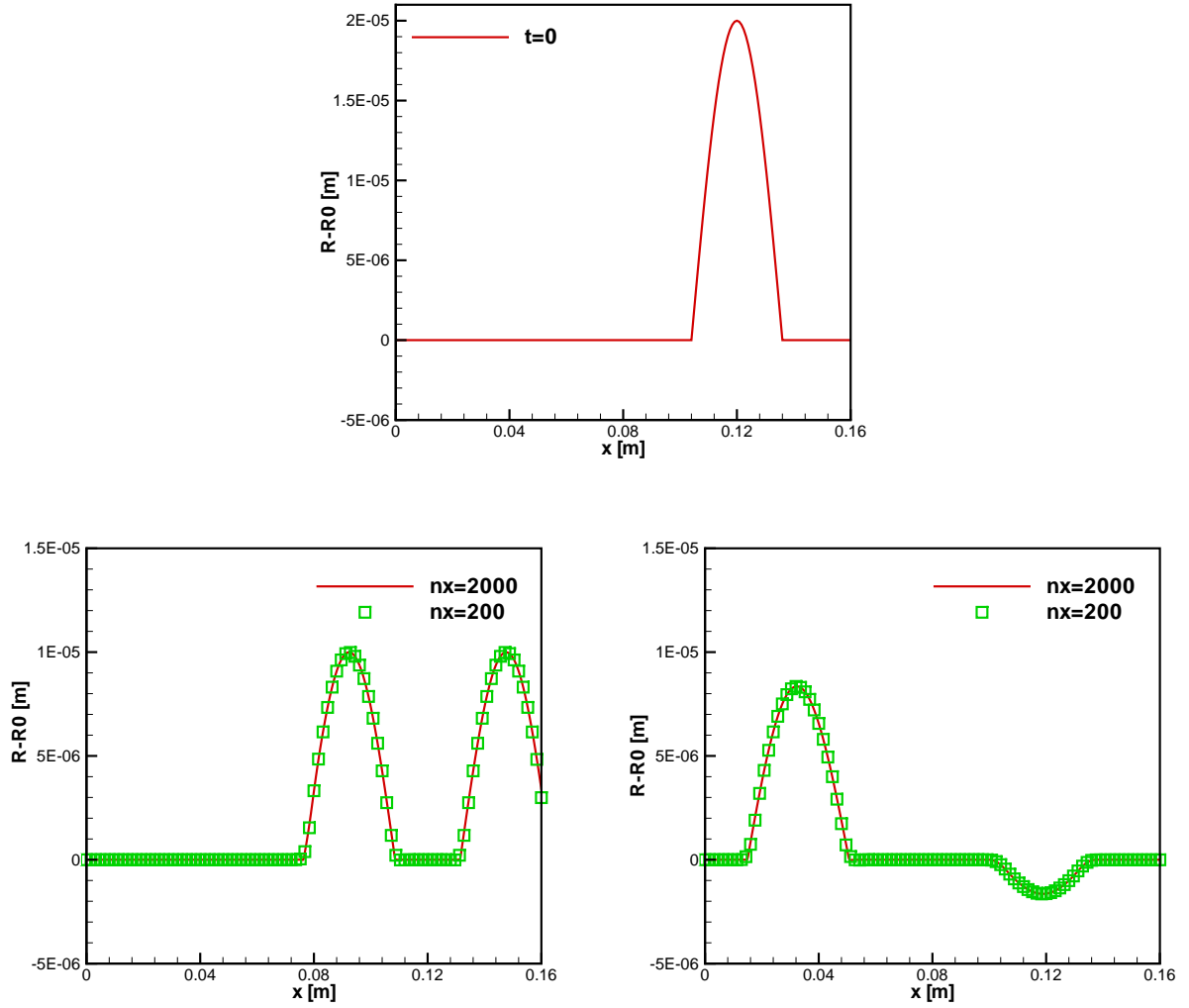


Fig. 4: The numerical solutions of the propagation of a pulse to an expansion in Section 3.4 with 200 cells. The errors $R - R_0$ at $t = 0$ s (upper), $t = 0.002$ s (lower left) and $t = 0.006$ s (lower right).

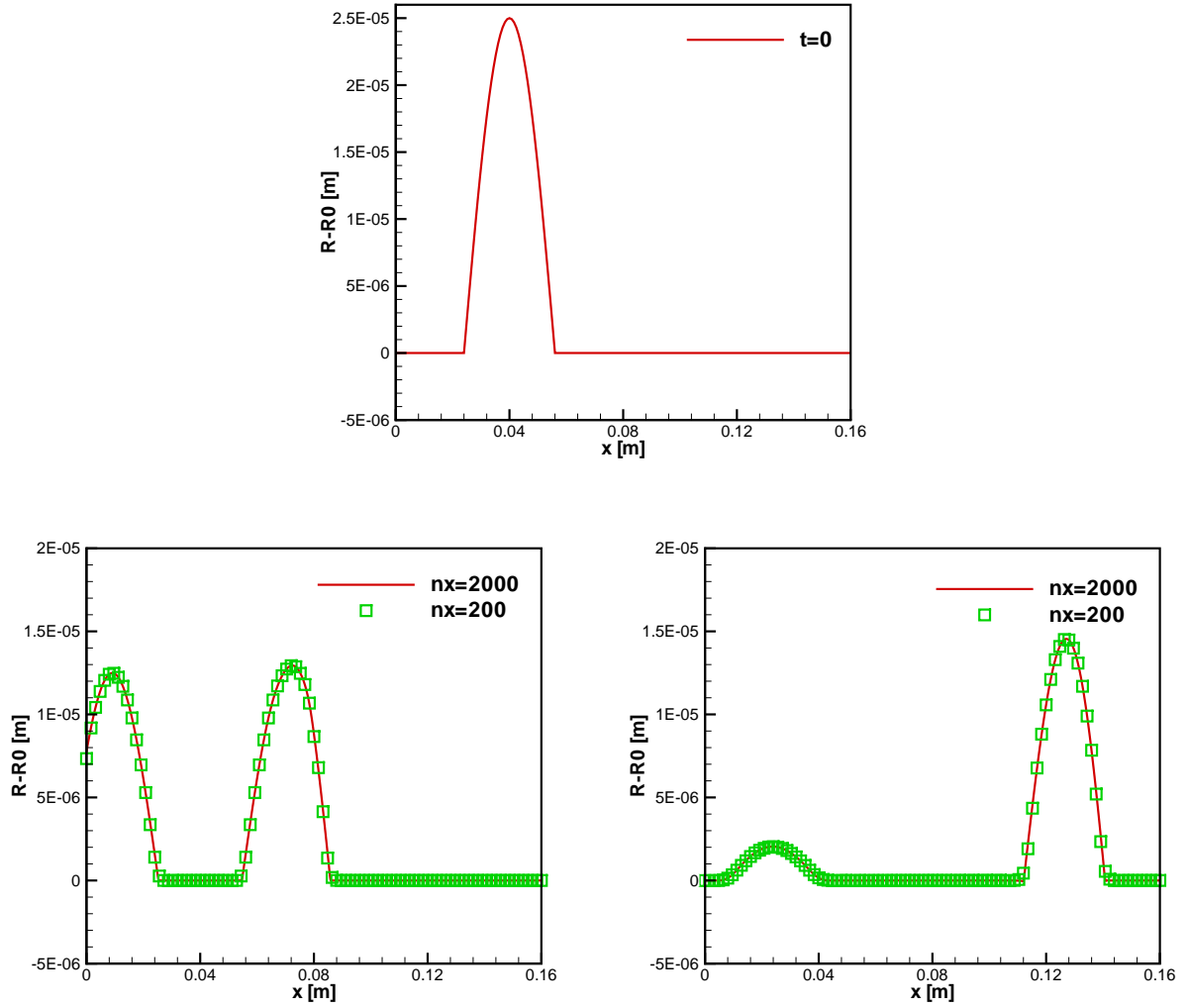


Fig. 5: The numerical solutions of the propagation of a pulse from an expansion in Section 3.5 with 200 cells. The errors $R - R_0$ at $t = 0$ s (upper), $t = 0.002$ s (lower left) and $t = 0.006$ s (lower right).

3.6. Wave damping

In this last test case, we look at the viscous damping term in the linearized momentum equation. This is the analogue of the Womersley [36] problem, we consider a periodic signal at the inflow with a constant section at rest. We consider the following model coupled with the linear friction term

$$\begin{cases} \partial_t A + \partial_x Q = 0, \\ \partial_t Q + \partial_x \left(\frac{Q^2}{A} + \frac{k}{3\rho\sqrt{\pi}} A^{\frac{3}{2}} \right) = \frac{kA}{\rho\sqrt{\pi}} \partial_x (\sqrt{A_0}) - C_f \frac{Q}{A}, \end{cases} \quad (24)$$

where $C_f = 8\pi\nu$ with ν being the blood viscosity. We consider this example on the computational domain $[0, 3]$ subject to the given initial conditions

$$\begin{cases} A(x, 0) = \pi R_0^2, \\ Q(x, 0) = 0, \end{cases}$$

accompanied by the following parameters: $k = 1 \times 10^8 \text{ Pa/m}$, $\rho = 1060 \text{ kg/m}^3$, $R_0 = 4 \times 10^{-3} \text{ m}$. We solve this example up to $t = 25 \text{ s}$.

Subsequently, we obtain a damping wave in the domain [25]

$$Q(t, x) = \begin{cases} 0 & \text{if } k_r x > \omega t, \\ Q_{\text{amp}} \sin(\omega t - k_r x) e^{k_i x} & \text{if } k_r x \leq \omega t, \end{cases} \quad (25)$$

with

$$\begin{aligned} k_r &= \left[\frac{\omega^4}{c_0^4} + \left(\frac{\omega C_f}{\pi R_0^2 c_0^2} \right)^2 \right]^{\frac{1}{4}} \cos \left(\frac{1}{2} \arctan \left(-\frac{C_f}{\pi R_0^2 \omega} \right) \right), \\ k_i &= \left[\frac{\omega^4}{c_0^4} + \left(\frac{\omega C_f}{\pi R_0^2 c_0^2} \right)^2 \right]^{\frac{1}{4}} \sin \left(\frac{1}{2} \arctan \left(-\frac{C_f}{\pi R_0^2 \omega} \right) \right), \\ \omega &= 2\pi/T_{\text{pulse}} = 2\pi/0.5 \text{ s}, \\ c_0 &= \sqrt{\frac{k\sqrt{A_0}}{2\rho\sqrt{\pi}}} = \sqrt{\frac{kR_0}{2\rho}}. \end{aligned}$$

For the boundary conditions, we impose the incoming discharge

$$Q_b(t) = Q_{\text{amp}} \sin(\omega t) \text{ m}^3/\text{s},$$

at $x = 0 \text{ m}$ with $Q_{\text{amp}} = 3.45 \times 10^{-7} \text{ m}^3/\text{s}^3$ being the amplitude of the inflow discharge. As the flow is subcritical, the discharge is imposed at the outflow boundary, thanks to (25) at the right boundary $x = 3 \text{ m}$.

In Fig. 6, we present the numerical results against the exact solutions at $t = 25$ s with different C_f . It is obvious that the numerical solutions are in good agreement with the exact solutions and are comparable with those in [25].

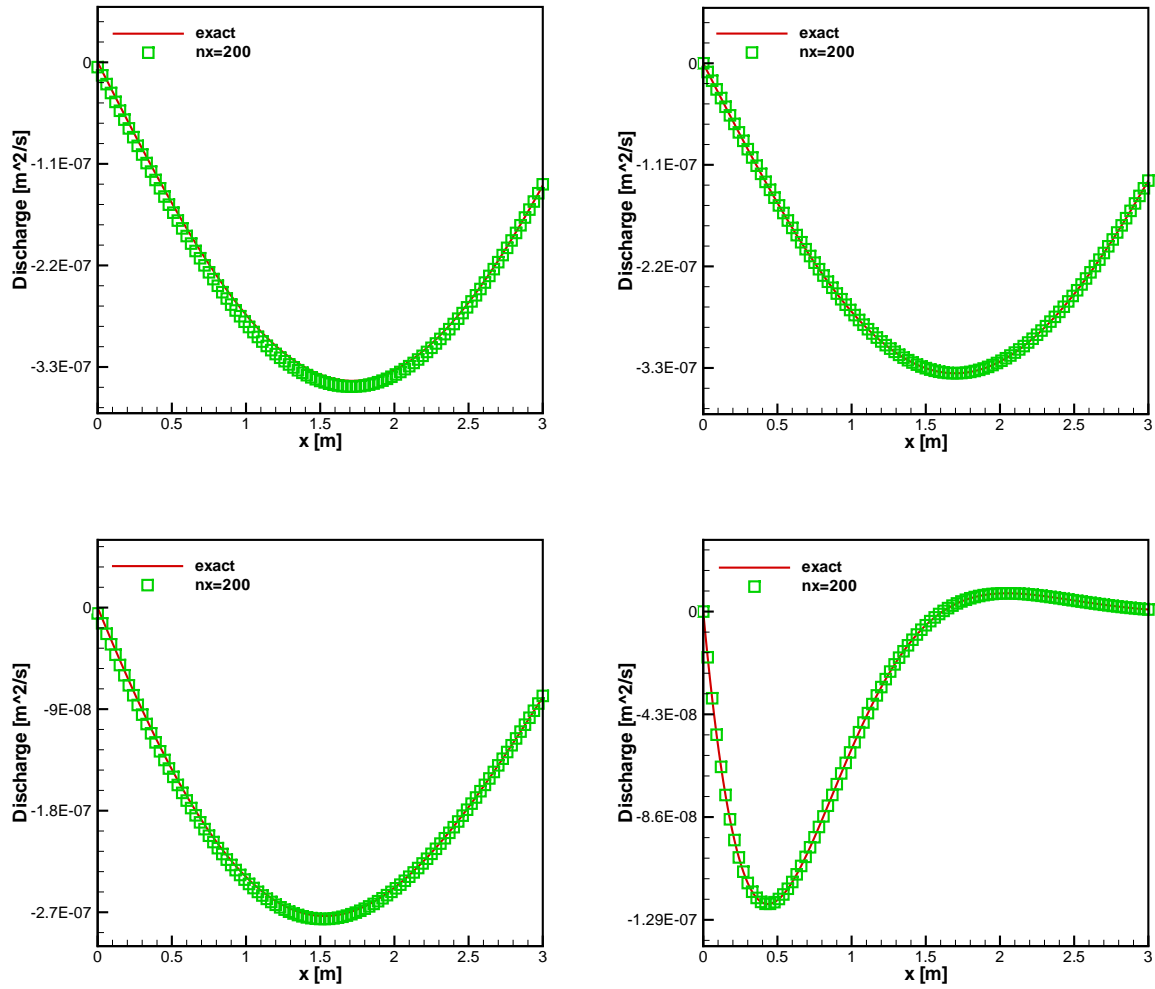


Fig. 6: The numerical solutions of the propagation of a pulse to and from an expansion in Section 3.6 with 200 cells at $t = 25$ s. The damping of a discharge wave with $C_f = 0$ (upper left), $C_f = 0.000022$ (upper right), $C_f = 0.000202$ (lower left) and $C_f = 0.005053$ (lower right).

4. Conclusions

In this paper, we have presented a well-balanced finite difference WENO scheme to solve the blood flow model. A special splitting of the source term allows us to design specific approximations such that the resulting WENO scheme maintains the well-balanced property for steady state solutions, and at the same time keeps their original high order accuracy and essentially non-oscillatory property for general solutions. Extensive numerical examples are given to demonstrate the well-balanced property, high order accuracy, and steep shock transitions of the proposed numerical scheme. The approach is quite general and can be adapted to high order finite volume schemes and discontinuous Galerkin finite element methods, which constitutes an ongoing work.

Acknowledgements

The research of the second author is supported by the National Natural Science Foundation of P.R. China (No. 11201254, 11401332) and the Project for Scientific Plan of Higher Education in Shandong Province of P.R. China (No. J12LI08). This work was partially performed at the State Key Laboratory of Science/Engineering Computing of P.R. China by virtue of the computational resources of Professor Li Yuan's group. The first author is also thankful to Professor Li Yuan for his kind invitation.

References

- [1] L. Formaggia, D. Lamponi, M. Tuveri, A. Veneziani. Numerical modeling of 1D arterial networks coupled with a lumped parameters description of the heart. *Computer Methods in Biomechanics and Biomedical Engineering*, 9:273-288, 2006.
- [2] V.B. Kolachalama, N.W. Bressloff, P.B. Nair, C.P. Shearman. Predictive Haemodynamics in a one-dimensional human carotid artery bifurcation. Part I: application to stent design. *IEEE Transactions on Biomedical Engineering*, 54:802-812, 2007.

- [3] D. Xiu, S.J. Sherwin. Parametric uncertainty analysis of pulse wave propagation in a model of a human arterial network. *Journal of Computational Physics*, 226:1385-1407, 2007.
- [4] K.H. Parker. A brief history of arterial wave mechanics. *Medical and Biological Engineering and Computing*, 47:111-118, 2009.
- [5] A. Bermudez, M.E. Vazquez. Upwind methods for hyperbolic conservation laws with source terms. *Computers & Fluids*, 23:1049-1071, 1994.
- [6] J.M. Greenberg, A.Y. Leroux. A well-balanced scheme for the numerical processing of source terms in hyperbolic equations. *SIAM Journal on Numerical Analysis*, 33:1-16, 1996.
- [7] J.M. Greenberg, A.Y. Leroux, R. Baraille, A. Noussair. Analysis and approximation of conservation laws with source terms. *SIAM Journal on Numerical Analysis*, 34:1980-2007, 1997.
- [8] S. Noelle, Y.L. Xing, C.-W. Shu. High-Order Well-balanced Schemes. in: *Numerical Methods for Balance Laws* (G. Puppo and G. Russo eds). *Quaderni di Matematica*, 2010.
- [9] Y.L. Xing, C.-W. Shu, S. Noelle. On the advantage of well-balanced schemes for moving-water equilibria of the shallow water equations. *Journal of Scientific Computing*, 48:339-349, 2011.
- [10] R.J. LeVeque. Balancing source terms and flux gradients in high-resolution Godunov methods: the quasi-steady wave-propagation algorithm. *Journal of Computational Physics*, 146:346-365, 1998.
- [11] B. Perthame, C.A. Simeoni. Kinetic scheme for the Saint-Venant system with a source term. *Calcolo*, 38:201-231, 2001.

- [12] K. Xu. A well-balanced gas-kinetic scheme for the shallow-water equations with source terms. *Journal of Computational Physics*, 178:533-562, 2002.
- [13] E. Audusse, F. Bouchut, M.O. Bristeau, R. Klein, B. Perthame. A fast and stable well-balanced scheme with hydro- static reconstruction for shallow water flows. *SIAM Journal on Scientific Computing*, 25:2050-2065, 2004.
- [14] Y.L. Xing, C.-W. Shu. High order finite difference WENO schemes with the exact conservation property for the shallow water equations. *Journal of Computational Physics*, 208:206-227, 2005.
- [15] Y.L. Xing, C.-W. Shu. A survey of high order schemes for the shallow water equations. *Journal of Mathematical Study*, 47:221-249, 2014.
- [16] S. Noelle, Y.L. Xing, C.-W. Shu. High-order well-balanced finite volume WENO schemes for shallow water equation with moving water. *Journal of Computational Physics*, 226:29-58, 2007
- [17] Y.L. Xing. Exactly well-balanced discontinuous Galerkin methods for the shallow water equations with moving water equilibrium. *Journal of Computational Physics*, 257:536-553, 2014.
- [18] F.Bouchut, T.Morales. A subsonic-well-balanced reconstruction scheme for shallow water flows. *SIAM Journal on Numerical Analysis*, 48:1733-1758, 2010.
- [19] C.T. Tian, K. Xu, K.L. Chan, L.C. Deng. A three-dimensional multidimensional gas-kinetic scheme for the navier-stokes equations under gravitational fields. *Journal of Computational Physics*, 226:2003-2027, 2007.
- [20] K. Xu, J. Luo, S. Chen. A well-balanced kinetic scheme for gas dynamic equations under gravitational field. *Advances in Applied Mathematics and Mechanics*, 2:200-210, 2010.

- [21] J. Luo, K. Xu, N. Liu. A well-balanced symplecticity-preserving gas-kinetic scheme for hydrodynamic equations under gravitational field. *SIAM Journal on Scientific Computing*, 33:2356-2381, 2011.
- [22] R. Kappeli, S. Mishra. Well-balanced schemes for the euler equations with gravitation. *Journal of Computational Physics*, 259:199-219, 2014.
- [23] Y.L. Xing, C.-W. Shu. High order well-balanced WENO scheme for the gas dynamics equations under gravitational fields. *Journal of Scientific Computing*, 54:645-662, 2013
- [24] G. Li, Y.L. Xing. Well-balanced discontinuous Galerkin methods for the Euler equations under gravitational fields. *Journal of Scientific Computing*, DOI: 10.1007/s10915-015-0093-5.
- [25] O. Delestre, P.Y. Lagrée. A ‘well-balanced’ finite volume scheme for blood flow simulation. *International Journal for Numerical Methods in Fluids*, 72:177-205, 2013.
- [26] O. Delestre, C. Lucas, P.-A. Ksinant, F. Darboux, C. Laguerre, T.N.T. Vo, F. James, S. Cordier. SWASHES: a compilation of Shallow Water Analytic Solutions for Hydraulic and Environmental Studies. *International Journal for Numerical Methods in Fluids*, 72:269-300, 2013.
- [27] M. Wibmer. One-dimensional simulation of arterial blood flow with applications. PhD Thesis, eingereicht an der Technischen Universität Wien, Fakultät für Technische Naturwissenschaften und Informatik, January, 2004.
- [28] N. Cavallini, V. Caleffi, V. Coscia. Finite volume and WENO scheme in one-dimensional vascular system modelling. *Computers and Mathematics with Applications*, 56:2382-2397, 2008.
- [29] N. Cavallini, V. Coscia. One-dimensional modelling of venous pathologies: finite volume and WENO schemes. In *Advances in Mathematical Fluid Mechanics*, Rannacher R, Sequeira A (eds). Springer: Berlin Heidelberg, 2010.

- [30] L.O. Müller, C. Parés, E.F. Toro. Well-balanced high-order numerical schemes for one-dimensional blood flow in vessels with varying mechanical properties. *Journal of Computational Physics*, 242:53-85, 2013.
- [31] J. Murillo, P. García-Navarro. A Roe type energy balanced solver for 1D arterial blood flow and transport. *Computers & Fluids*, 117:149-167, 2015.
- [32] G. Jiang, C.-W. Shu. Efficient implementation of weighted ENO schemes. *Journal of Computational Physics*, 126:202-228, 1996.
- [33] C.-W. Shu. Essentially non-oscillatory and weighted essentially non-oscillatory schemes for hyperbolic conservation laws, NASA/CR-97-206253, ICASE Report NO.97-65.
- [34] C.-W. Shu. High order weighted essentially nonoscillatory schemes for convection dominated problems. *SIAM Review*, 51:82-126, 2009.
- [35] C.-W. Shu, S. Osher. Efficient implementation of essentially non-oscillatory shock-capturing schemes. *Journal of Computational Physics*, 77:439-471, 1988.
- [36] Womersley J. On the oscillatory motion of a viscous liquid in thin-walled elastic tube: I. *Philosophical Magazine*, 46:199-221, 1955.